



70%

of surveyed scientists admitted that they could not replicate someone else's research.<sup>1</sup>

50%

admitted that they couldn't replicate their own research.<sup>1</sup>



## Stem Cells Demand Reproducibility.

PHCbi brand Cell-IQ™ CO<sub>2</sub> and O<sub>2</sub> incubators are designed to deliver reproducibility critical to stem cell research and regenerative medicine.

Your desired temperature and gas concentrations replicate the *in vivo* model of any cell culture environment with precision and predictability. Our SafeCell™ and inCu-saFe® technologies protect your work *in vitro*. Learn more at [www.phcd.com/us/biomedical/cell-culture-incubators](http://www.phcd.com/us/biomedical/cell-culture-incubators).



Select from eight models including your choice of high heat or H<sub>2</sub>O<sub>2</sub> decontamination with CO<sub>2</sub> or CO<sub>2</sub>/O<sub>2</sub> control.


### PHC Corporation of North America

PHC Corporation of North America  
1300 Michael Drive, Suite A, Wood Dale, IL 60191  
Toll Free USA (800) 858-8442, Fax (630) 238-0074  
[www.phcd.com/us/biomedical](http://www.phcd.com/us/biomedical)

<sup>1</sup>) Baker, Monya. "1,500 scientists lift the lid on reproducibility." Nature, no. 533 (May 26, 2016): 452-54. doi:10.1038/533452a.

**PHC Corporation of North America** is a subsidiary of PHC Holdings Corporation, Tokyo, Japan, a global leader in development, design and manufacturing of laboratory equipment for biopharmaceutical, life sciences, academic, healthcare and government markets.

# Functional dosing of mesenchymal stromal cell-derived extracellular vesicles for the prevention of acute graft-versus-host-disease

Giada Dal Collo<sup>1</sup>  | Annalisa Adamo<sup>1</sup> | Alessandro Gatti<sup>1</sup> | Edoardo Tamellini<sup>1</sup> | Riccardo Bazzoni<sup>1</sup> | Paul Takam Kanga<sup>1,2</sup> | Cristina Tecchio<sup>1</sup> | Francesca Maria Quaglia<sup>1</sup> | Mauro Krampera<sup>1</sup>

<sup>1</sup>Stem Cell Research Laboratory, Section of Hematology, Department of Medicine, University of Verona, Verona, Italy

<sup>2</sup>EA4340-BCOH, Biomarker in Cancerology and Onco-Haematology, UVSQ, Université Paris Saclay, Boulogne-Billancourt, France

## Correspondence

Mauro Krampera, MD, PhD, Stem Cell Research Laboratory, Section of Hematology, Department of Medicine, University of Verona, Policlinico G.B. Rossi, P.le L. Scuro, 10, 37134 Verona, Italy.  
Email: mauro.krampera@univr.it

## Funding information

Fondazione Cassa di Risparmio di Verona Vicenza Belluno e Ancona

## Abstract

Graft-vs-host-disease (GvHD) is currently the main complication of allogeneic hematopoietic stem cell transplantation. Mortality and morbidity rates are particularly high, especially in steroid-refractory acute GvHD (aGvHD). Immune regulatory human bone marrow mesenchymal stromal cells (hMB-MSCs) represent a therapeutic approach to address this issue. Unfortunately, their effect is hardly predictable in vivo due to several variables, that is, MSC tissue origin, concentration, dose number, administration route and timing, and inflammatory status of the recipient. Interestingly, human bone marrow MSC-derived extracellular vesicles (hBM-MSC-EVs) display many of the hBM-MSC immunoregulatory properties due to their content in paracrine factors that greatly varies according to the collection method. In this study, we focused on the immunological characterization of hBM-MSC-EVs on their capability of inducing regulatory T-cells (T-regs) both in vitro and in a xenograft mouse model of aGvHD. We correlated these data with the aGvHD incidence and degree following hBM-MSC-EV intravenous administration. Thus, we first quantified the EV immunomodulation in vitro in terms of EV immunomodulatory functional unit (EV-IFU), that is, the lowest concentration of EVs leading in vitro to at least threefold increase of the T-regs compared with controls. Second, we established the EV therapeutic dose in vivo (EV-TD) corresponding to 10-fold the in vitro EV-IFU. According to this approach, we observed a significant improvement of both mouse survival and control of aGvHD onset and progression. This study confirms that EVs may represent an alternative to whole MSCs for aGvHD prevention, once the effective dose is reproducibly identified according to EV-IFU and EV-TD definition.

## KEYWORDS

extracellular vesicles, GvHD, immunomodulation, mesenchymal stromal cells, MSCs

## 1 | INTRODUCTION

The main complication of allogeneic hematopoietic stem cell transplantation (Allo-HSCT) is graft-vs-host-disease (GvHD), a donor T-cell-mediated

alloreactive inflammatory disease affecting 20%-70% of patients.<sup>1-4</sup> GvHD, initially classified as acute (aGvHD) and chronic (cGvHD) on the basis of the onset time after Allo-HSCT (aGvHD <100 days, cGvHD >100 days), is now described according to a new scoring system based on the clinical signs and symptoms and pathogenesis.<sup>5-8</sup> Clinical manifestations of aGvHD involve the skin, the gastrointestinal tract, and the liver and include maculopapular erythema, gastrointestinal symptoms (abdominal cramps and diarrhea), and cholestatic hepatitis, whereas cGvHD can virtually affect any tissue/organ.<sup>9,10</sup> Immunosuppression with steroids is currently the first-line therapy for aGvHD.<sup>11</sup> However, refractoriness to steroid-based protocols characterizes about 30% of the patients; aggressive immunosuppressive treatments or anti-inflammatory agents are effective in a variable proportion of steroid-refractory patients, but the overall survival is generally poor, with only a few long-term survivors.<sup>12,13</sup> Consequently, alternative approaches, such as the administration of mesenchymal stromal cells (MSCs), have been proposed in the last decade for refractory aGvHD treatment.<sup>14-17</sup> In 2004, the first successful use of MSCs was reported in severe aGvHD treatment.<sup>14</sup> Since then, several clinical and preclinical studies have been performed with controversial results due to the heterogeneity in the treatment schedules (ie, MSC concentration, dose number, administration route, and timing) and to other factors, such as MSC tissue origin and inflammatory status of the recipient.<sup>17-21</sup> Similar controversial results and side effects (eg, pulmonary embolization) were shown by preclinical studies performed in mouse models.<sup>22-24</sup>

Human bone marrow-derived MSCs (hBM-MSCs) are a heterogeneous fibroblast-like cell population, including both multipotent stem cells with the ability to form bone, cartilage, and adipose tissue *in vitro*<sup>25</sup> and stromal cell components that regulate hematopoietic stem cell niche through specific cell-to-cell interactions and soluble factor release.<sup>26</sup> In 2006, the International Society for Cell & Gene Therapy (ISCT) established the minimal criteria to define MSCs, that is, the ability to grow as adherent cells, the membrane surface expression of a marker combination pattern, including CD73, CD90, and CD105 together with the lack of CD14, CD31, CD34, CD45, and HLA-DR expression, and the ability to differentiate into adipocytes, osteoblasts, and chondrocytes.<sup>27</sup> A general functional feature of MSC population, both of stem cells and differentiating progenitors, is the acquisition of immunomodulatory properties toward cells of both innate and adaptive immunity, depending on the presence of inflammatory cytokines in the microenvironment, such as interferon (IFN)- $\gamma$ , tumor necrosis factor (TNF)- $\alpha$ , and interleukin (IL)-1 $\alpha$  or  $\beta$ .<sup>28</sup>

The immunoregulatory functions of MSCs can be mediated not only by direct cell-to-cell contact, but also in a paracrine manner, mostly through the release of extracellular vesicles (EVs).<sup>29,30</sup> EVs are spherical membrane-coated particles consisting of a lipid bilayer surrounding a glycoproteic and nucleic acid content.<sup>31</sup> According to their size and content, EVs are classified as microvesicles, exosomes, and apoptotic bodies, each with different biological effects.<sup>31,32</sup> Our group has recently shown *in vitro* that hBM-MSC-EVs are capable of mediating immunoregulatory effects towards different immune effector cells (IECs) by inhibiting B- and NK-cell proliferation and increasing

### Significance statement

A number of extracellular vesicle (EV) pools have been used in the study obtained from different donor-derived bone marrow mesenchymal stromal cells expanded in human platelet lysate-conditioned medium, displaying *in vitro* the same reproducible immune regulatory activity, regardless of their protein concentration. The effectiveness of these EV pools was then tested *in vivo* in a xenogeneic mouse model of severe acute graft-vs-host-disease (aGvHD). Thus, the functional parameters were defined *in vitro* and *in vivo* to measure and predict the capability of EVs to improve mouse survival and control of aGvHD progression.

CD4<sup>+</sup> T-cell population, thus suggesting a possible involvement of T-regulatory cells (T-regs).<sup>30,33</sup> T-regs, a subset of CD4<sup>+</sup> T cells expressing the IL-2 alpha-chain-receptor (CD25) and the nuclear transcription factor Forkhead box P3 (FoxP3), can suppress proliferation and effector functions in T-, B-, NK-cells, as well as antigen-presenting cells<sup>34</sup>; consequently, T-reg-based cell therapies could be effective the treatment of various autoimmune diseases, including GvHD.<sup>35</sup> The same inflammatory cytokines that trigger immunoregulatory functions of hBM-MSCs and therefore hBM-MSC-EVs, such as TNF- $\alpha$  and IFN- $\gamma$ , also promote T-reg activation and inhibitory functions, thus enhancing the protection towards GvHD-associated tissue injury in mouse models of Allo-HSCT.<sup>36,37</sup> Consequently, hBM-MSC-EVs may represent a potential therapeutic tool for aGvHD treatment, provided some safety requirements for clinical use are satisfied.<sup>38</sup> Among them, the use of heterologous supplements for hBM-MSC culture and EV collection, such as fetal bovine serum (FBS), should be avoided to minimize the risk of infectious contaminants, such as mycoplasma, viruses, endotoxins, or prions.<sup>39</sup> To this aim, human platelet lysate (hPL) has been clinically tested for safety in many protocols of human MSC *ex vivo* culture and expansion.<sup>39,40</sup> hPL contains a wide variety of growth and angiogenic factors, including platelet-derived growth factor (PDGF)-AA, PDGF-AB, and PDGF-BB, transforming growth factor (TGF)- $\beta$ 1 and TGF- $\beta$ 2, epidermal growth factor, vascular endothelial growth factor, basic-fibroblast growth factor, brain-derived neurotrophic factor, and hepatocyte growth factor.<sup>40</sup> Thus, hPL seems to be a suitable substitute of FBS, in terms of reproducibility and safety, for *ex vivo* MSC-EV production for preclinical and clinical purposes.<sup>39,40</sup>

After systemic injection, the half-life of circulating EVs is approximately 2 minutes, but EVs have been detected after 48 hours in lungs, liver, spleen, and pancreas,<sup>41</sup> thus suggesting a potential long-term therapeutic effect once administered intravenously. On this basis, several studies suggest a potential therapeutic role of EVs in inflammatory and autoimmune diseases, such as aGvHD<sup>38</sup>; however, the lack of standardized treatment protocols still represents a major hurdle to clearly demonstrate the *in vivo* effectiveness of EV administration.

In this study, we first assessed the best culture conditions to obtain hBM-MSC-EVs by comparing cell expansion and regulatory properties toward different IECs with either FBS- or hPL-supplemented culture media. Then, we evaluated both in vitro and in vivo in a mouse xenograft model of aGvHD, the therapeutic potential of hPL-hBM-MSC-EVs. Thus, we could confirm that EVs may represent a valid alternative to whole MSC administration for aGvHD treatment. In addition, the definition of EV immunomodulatory functional unit (EV-IFU) in vitro and EV therapeutic dose in vivo (EV-TD) may help to standardize the identification of the EV effective dose for clinical purposes.

## 2 | MATERIALS AND METHODS

### 2.1 | Cell culture

MSCs were isolated from BM aspirates of healthy donors (after informed consent, approved by Ethical Committee of Azienda Ospedaliera Universitaria Integrata Verona; N.1828, May 12, 2010, "Institution of cell and tissue collection for biomedical research in Onco-Hematology"), expanded and characterized as already described.<sup>30,42</sup> hBM-MSCs were cultured in a minimal essential medium supplemented with either 10% FBS, FBS-hBM-MSCs, or 5%-8% hPL<sup>40</sup> (first and following passages, respectively) and heparin sodium (3 IU/mL), hPL-hBM-MSCs, 1% penicillin-streptomycin, and 2% L-Glutamine (Sigma-Aldrich). hPL was obtained from a platelet-rich plasma pool of 15 healthy donors, following the standardized clinical-grade procedures already described (40) according to the Italian ministerial regulation "DM November 2, 2019," thus minimizing the variability of the process. Samples of hPL were stored at  $-80^{\circ}\text{C}$  for 16 hours, and then centrifuged twice at 4000g for 20 minutes. Prior to medium preparation, FBS and hPL were depleted in EVs through ultracentrifugation as previously described.<sup>30</sup> To avoid any contamination of serum EVs, the EV-free medium was filtered by using a 0.2- $\mu\text{m}$  filter that removes the largest population of EVs. The absence of the smallest population of EVs (exosomes) was evaluated by FACS, assessing the negative expression of the well-established exosome markers in EV-depleted culture media. In addition, the hPL-MSCs used in our work were routinely tested for mycoplasma contamination, which was excluded. hBM-MSCs at 80% confluence were treated (primed hBM-MSCs) or not (resting hBM-MSCs) for 48 hours with 10 ng/mL IFN- $\gamma$  and 15 ng/mL TNF- $\alpha$  (R&D Systems) to induce inflammatory priming. Human peripheral blood mononuclear cells (PBMCs) were isolated using Lymphoprep (Stemcells Technologies) and used for IEC isolation through immunomagnetic negative selection (Miltenyi Biotec) with at least 95% cell purity. For immunological assay, IECs were activated through specific stimuli (T cells: 0.5  $\mu\text{g}/\text{mL}$  of anti-CD3 and anti-CD28 (PeliCluster); B cells: 2.5  $\mu\text{g}/\text{mL}$  CPG ODN (InvivoGen), 50 ng/mL CD40L (R&D systems), 5  $\mu\text{g}/\text{mL}$  MAB 50 (R&D systems), 20 U/mL IL-2 (Miltenyi Biotec), and 2  $\mu\text{g}/\text{mL}$  FAB (IgG, IgM, IgA) (Jackson ImmunoResearch); NK-cells: 100 U/mL IL-2 (Miltenyi Biotec).

### 2.2 | FACS analysis

The identity of hBM-MSCs was checked according to the ISCT guidelines and characterized for the presence of mesenchymal markers, that is, CD73-PE, CD90-PE, and CD105-PE (BD Bioscience); the absence of endothelial and hematopoietic markers, that is, CD14-PE, CD31-PE, CD34-PE, and CD45-PE (BD Bioscience); as well as immunological markers, that is, HLA-ABC-PE and HLA-DR-PE (BD Bioscience). The inflammatory immunophenotype of hBM-MSCs was established by the detection of inflammatory markers, including CD54-PE, CD80-PE, CD86-PE, CD106 PE, HLA-ABC-PE, HLA-DR-PE (BD Bioscience), CD273-APC, CD274-PE, and CD279-PE (Biolegend). PBMCs were characterized using CD3-FITC, CD16/56-PE, CD45-PerCP, CD19-APC, CD4-APC-H7, and CD8-PECy7 (BD Bioscience), whereas cell viability was assessed by using TO-PRO-3-iodide (Life Technologies) or Viability Fixable Dyes-V500 (Miltenyi Biotec). T-reg immunophenotype was assessed by labeling the samples with CD3-V450, CD4-PerCP, CD8-APC-Cy7, CD25-FITC, CD127-PE-Cy7, FoxP3-APC, Viability Fixable Dyes-V500 (Miltenyi Biotec), and the experiments were performed according to manufacturer's instructions of FoxP3 Staining Buffer Set (Miltenyi Biotec). The gating strategy was performed on viable CD3<sup>+</sup> and CD4<sup>+</sup> T cells and then on CD25<sup>+</sup>CD127<sup>low</sup> cells to define T-reg phenotype. All data were collected through flow cytometry (FACS Canto II, BD Bioscience) and analyzed using FlowJo software (TreeStar).

### 2.3 | Proliferation and cytotoxicity assay

To study cell proliferation, activated IECs were labeled with 5  $\mu\text{M}$  carboxy-fluorescein-succinimidyl-ester (CFSE) (Life Technologies), as previously described,<sup>43</sup> and co-cultured with resting or primed-hBM-MSCs for 4 days (B cells) or 6 days (T and NK cells) at the MSCs:IECs ratio of 1:10 and 1:1 (T cells and B, NK cells, respectively). Cytotoxicity was analyzed through DELFIA cell cytotoxicity kit. The experiments were performed according to the manufacturer's instructions (Perkin Elmer), using activated NK-cells for 48 hours and co-cultured with BATDA-labeled hBM-MSCs at the NK-cells:hBM-MSCs ratios of 1:1, 5:1, 15:1, 25:1 at  $37^{\circ}\text{C}$  for 3 hours. Fluorescence was measured at 615 nm using VICTORTMX4.

### 2.4 | Purification, characterization, and quantification of hBM-MSC-EVs

Following cell expansion in EV-free conditioned medium, hBM-MSC-EVs were isolated from hBM-MSCs supernatant by ultracentrifugation, as previously described.<sup>30</sup> EV pools were obtained by mixing EVs isolated from 5 hPL-hBM-MSC donors, with the purpose to reduce inter-individual variability. Isolated EVs were resuspended in phosphate-buffered saline (PBS) and stored at  $-80^{\circ}\text{C}$ . EV protein quantification was performed through BCA (bicinchoninic acid) Protein Assay (Thermo Fisher Scientific). Particle size was evaluated by dynamic light scattering (DLS) measurements using a Zetasizer Nano



ZS (Malvern Instruments, 4 mV He-Ne laser,  $\lambda = 633 \text{ nm}$ ,  $\theta = 173^\circ$ ). The DLS method can measure particles ranging from 1 nm to 6  $\mu\text{m}$ . The eventual presence of membrane fragments with different size and shape can be easily detected in the hydrodynamic diameter distribution plots of the particle's suspension analyzed. To assess the expression pattern of surface markers, 10  $\mu\text{g}$  of EVs were analyzed using the MACSPlex Exosome Kit (Miltenyi Biotec), a multiplex bead-based platform allowing the detection of 37 surface epitopes. Samples were analyzed with FACS Canto II (BD Biosciences).

## 2.5 | Transmission electron microscopy

Stored EV samples were thawed on ice. Ten microliters of EVs were pipetted on an ultra-thin carbon coated copper grid (CF200H-Cu-UL, Electron Microscopy Sciences) for 5 minutes and the excess was removed by gentle blotting. The grid was previously treated with UV light for 15 minutes. The grid was placed on one drop of UranylLess solution (Electron Microscopy Sciences) for 1 second, gently blotted, and then put on a second drop for 2 minutes. The excess of solution was removed by blotting. The grid was air-dried. Grid was visualized on a Morgagni 268D (FEI Philips) transmission electron microscope at 80 kV. Images were taken with MegaView G3 camera and RADIUS software (both from EMSIS GmbH).

## 2.6 | Xenograft mouse model

NOD/Shi-scid/IL-2R $\gamma$ null (NOG) mice were purchased from Taconic (Germantown, New York) and kept in pathogen-free conditions in the animal facility of the Interdepartmental Centre of Experimental Research Service (CIRSAL) of the University of Verona, as approved by the Italian Minister of Health. To induce aGvHD,  $1 \times 10^6$  human PBMCs/g (PBS-only as control) were injected via tail vein into 8- to 12-week-old female mice previously irradiated with 1.2 Gy from a  $^{137}\text{Cs}$  source. The PBMCs derived from different batches, one for each in vivo experiment ( $n = 5$ , from PBMCs 1 to PBMCs 5). Mice were randomized and split into two treatment groups: (a) EV-UT mice (untreated aGvHD mice) receiving PBS i.v. and (b) EV-TD mice

(treated aGvHD mice) receiving EV-TD i.v. at +1, +4, +7 days after PBMC injection. Mice were monitored daily until the end of experiments (day +30), evaluating the onset of aGvHD clinical symptoms, weight loss, and overall survival. Mice were ethically euthanized when either the weight loss was over 20% of the initial weight or the cumulative clinical score was 6 (Table 1).

## 2.7 | Evaluation of T-cell infiltration and T-reg induction in in vivo aGvHD model

Lung, liver, spleen, and kidney were collected from sacrificed aGvHD mice, and dissociated with 1 mM PBS EDTA, following the manufacturer's instructions of gentle MACS Dissociator (Miltenyi Biotec). BM was harvested through flushing, whereas peripheral blood (PB) was collected from retroorbital vein in tubes with heparin or D-Phenylalanyl-L-prolyl-L-arginine chloromethyl ketone (PPACK) (Sigma-Aldrich). PB samples were maintained at 4°C to avoid coagulation. To evaluate lymphocyte infiltration in mouse tissues and T-reg induction in PB, IECs and T-regs were analyzed by FACS Canto II (BD Biosciences). Splenomegaly was measured by the caliber, on day 15 after PBMC inoculation.

## 2.8 | ELISA assay

PB collection through retroorbital bleeding in aGvHD mice, previously anesthetized by isoflurane, was performed at +9 and +12 days. Plasma samples were obtained by centrifugation for 10 minutes at 2000g. Human cytokine levels (IFN- $\gamma$  and TNF- $\alpha$ ) in plasma samples were analyzed through Quantikine ELISA kit. The experiments were performed according to the manufacturer's instructions (R&D Systems). The levels of human cytokines were determined using VICTORTMX4 at 450 nm, and the concentrations reported in pg/mL.

## 2.9 | Statistics and image software

Statistical analysis was performed using GraphPad Prism software (La Jolla, California). Data were expressed as mean  $\pm$  standard error

**TABLE 1** Clinical scoring system used for aGvHD onset evaluation in NOG mice

Clinical score	0	0.5	1	1.5	2
Posture	Normal	Slight hunching	Moderate hunching but correct movement	Strong hunching and slightly impaired movement	Strong hunching and distinct impaired movement
Activity	Normal	Less movement than normal, easier to catch	Very little movement	Animal stay still but will move when touched	Animal has no activity also when touched
Fur	Normal	Slight ruffling on the neck	Slight ruffling on the neck, belly and back	Moderate ruffling all over the body	Matted Fur and color changing (yellowing)

Notes: Clinical scoring before aGvHD mouse euthanasia. Mice were ethically euthanized before the end of the experiment (day +30) when the cumulative clinical score was 6.

Abbreviation: aGvHD, acute graft-vs-host-disease.

means. Student's *t*-test was used to compare two groups, and one-way ANOVA followed by the Tukey's range test was applied to compare multiple groups. Mann-Whitney's test was used for noncoupled, nonparametric comparison. Differences in Kaplan-Meier survival curves were analyzed with the Log-rank (Mantel-Cox) test.  $P < .05$  was considered as statistically significant. Adobe Illustrator software (Adobe Inc.) was used to perform the 2D-protocol.

### 3 | RESULTS

#### 3.1 | Superiority of hPL-supplemented medium for hBM-MSC expansion and immunoregulatory studies

In line with the literature data,<sup>44</sup> five healthy donor-derived hBM-MSC samples were expanded by using either FBS- or hPL-supplemented culture media until the end of the cell expansion (day  $19 \pm 2$ ), and

consequently characterized according to the ISCT guidelines.<sup>27</sup> Even though hPL-hBM-MSCs showed a stronger expression of CD73, CD90, and HLA-ABC compared with FBS-hBM-MSCs, immunophenotypic pattern was similar for FBS- and hPL-hBM-MSCs (Figure S1A). Mesodermal differentiation was comparable with the two culture protocols (Figure S1B). Cell growth rate at day  $19 \pm 2$  was higher in hPL-hBM-MSCs, as assessed through total cell number at the first cell passage (p1) (Figure S1C), the clonogenicity (Figure S1D), and the population doubling (Figure S1E), thus confirming the superiority of the hPL-based medium to enhance hBM-MSC expansion. At p3, both FBS- and hPL-hBM-MSCs showed a normal karyotype (Figure S2A). Moreover, in hPL-hBM-MSCs no significant differences were observed in expression levels of some oncogenes, onco-suppressors, and cell cycle regulator genes, such as *C-MYC*, *hTERT*, *TP53*, and *CDKN1A*, between p0 and p1. *hTERT* was undetectable in the two kinds of hBM-MSCs (data not shown). After showing that hPL-supplemented medium did not influence functional and molecular characterization of hBM-MSCs, we focused on the

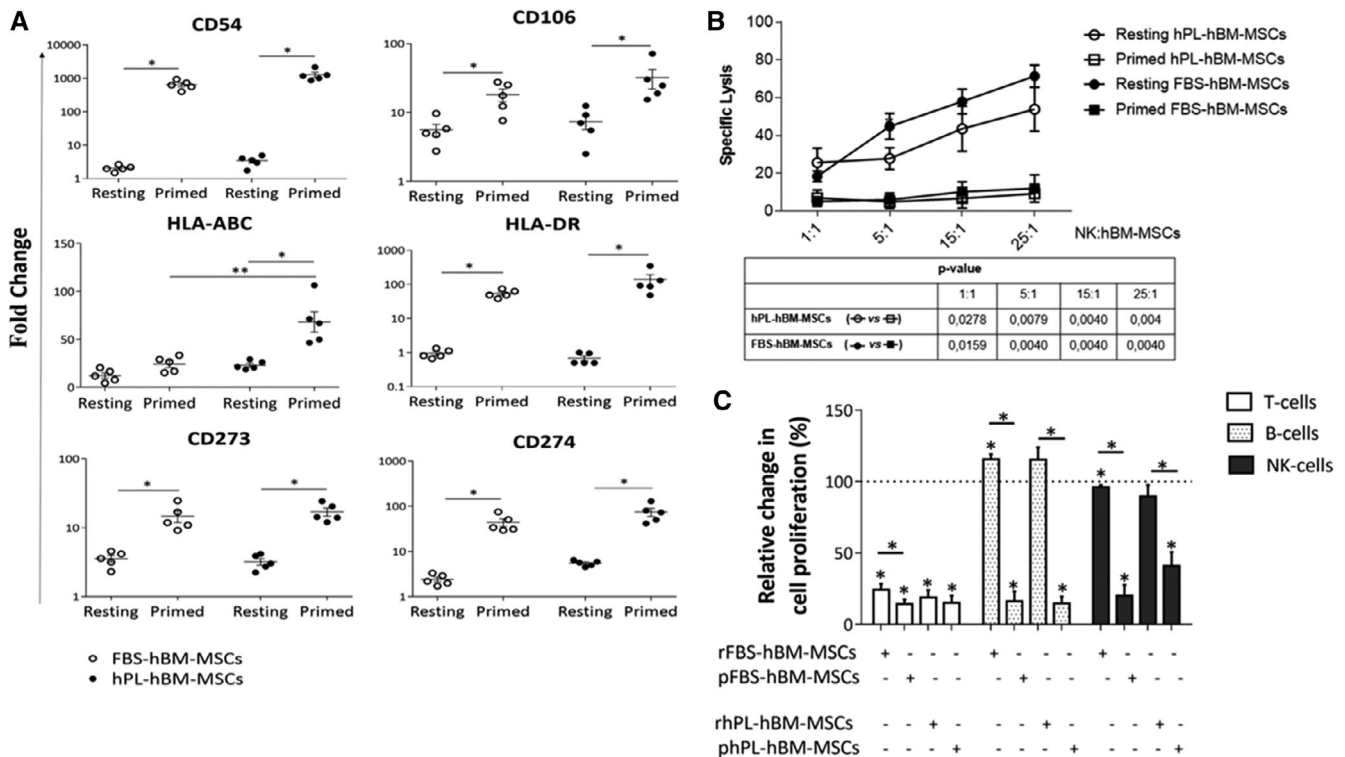


**FIGURE 1** Immunomodulatory properties of hBM-MSCs expanded in hPL-based culture medium. A, FBS- and hPL-hBM-MSCs were treated (primed hBM-MSCs) or not (resting hBM-MSCs) with IFN- $\gamma$  (10 ng/mL) and TNF- $\alpha$  (15 ng/mL) for 48 hours. The expression of surface markers (CD54, CD106, HLA-ABC, HLA-DR, CD274, CD273) was evaluated by FACS analysis. Results are represented as fold change expression of each specific marker compared with isotype control. Error bars represent mean  $\pm$  SEM of five independent experiments. Mann-Whitney test was used for statistical analysis. B, Both resting and primed FBS- and hPL-hBM-MSCs were incubated at different activated NK-cells:hBM-MSCs ratios (1:1, 5:1, 15:1, 25:1) for 3 hours. Data are represented as NK cell-specific lysis. Error bars represent mean  $\pm$  SEM of five independent experiments. Mann-Whitney test was used for statistical analysis. C, Activated IECs were co-cultured alone or in the presence of rhBM-MSCs or pBM-MSCs for 4 days (with B-cells) or 6 days (with T- and NK-cells) at the MSCs:IEC ratio of 1:10 and 1:1 (with T-cells and B-, NK-cells, respectively). Data are represented as percentage of relative proliferating cells. Error bars represent mean  $\pm$  SEM of five independent experiments. Mann-Whitney test was used for statistical analysis. \* $P < .05$ , \*\* $P < .01$ . FBS, fetal bovine serum; hBM-MSCs, human bone marrow-derived MSCs; hPL, human platelet lysate; IECs, immune effector cells; MSCs, mesenchymal stromal cells

immunological properties of hPL-BM-MSCs, demonstrating that hPL-hBM-MSCs were also capable of acquiring the inflammatory phenotype, that is, increased expression of CD54 (I-CAM), CD106 (V-CAM), HLA-DR (MHC-II), CD273 (PD-L2), and CD274 (PD-L1) (Figure 1A and S3A). In addition, hPL-BM-MSCs showed higher expression of HLA-ABC (MHC-I) following inflammatory priming (Figure 1A and S3A), compared with FBS-hBM-MSCs. Our data demonstrated that resting-hBM-MSCs displayed a partial sensitivity to NK cell-mediated lysis, which was prevented by inflammatory priming, without significant differences between FBS- and hPL-hBM-MSCs (Figure 1B), in line with previous reports.<sup>28</sup> We also found that resting hPL-hBM-MSCs inhibited T- and NK-cell proliferation and showed a trophic effect toward B cells. In contrast, both primed FBS- and hPL-hBM-MSCs inhibited more significantly T- and NK-cell proliferation and affected B cells although without significant differences (Figure 1C). Overall, our data showed that hPL-based expansion protocol did not affect hBM-MSC immunological properties and inhibitory functions, but it confers superiority in terms of expansion yield. As we have previously demonstrated that

hBM-MSC-EVs exhibit most of the properties of hBM-MSCs,<sup>32</sup> the hPL-based expansion protocol was chosen to obtain hBM-MSC-EVs for the further experiments.

### 3.2 | Characterization of EVs obtained from hPL-hBM-MSCs

Considering the potential capability of serum EV to influence cell behavior, we first assessed the absence of hPL-derived EVs in the EV-free medium. With this aim, hBM-MSC-EVs were isolated as pellet by ultracentrifugation and were washed repeatedly with PBS to eliminate any medium-derived protein contamination. In addition, we evaluated by FACS analysis the expression of the well-established exosome markers in EV-depleted and filtered hPL culture media. CD9, CD63, and CD81 resulted negative compared with hPL-MSC-EVs (Figure 2A). Our previous data showed that EVs from resting- and primed FBS-hBM-MSCs stored at  $-80^{\circ}\text{C}$  maintain their integrity, as revealed by DLS profile.<sup>33</sup> In

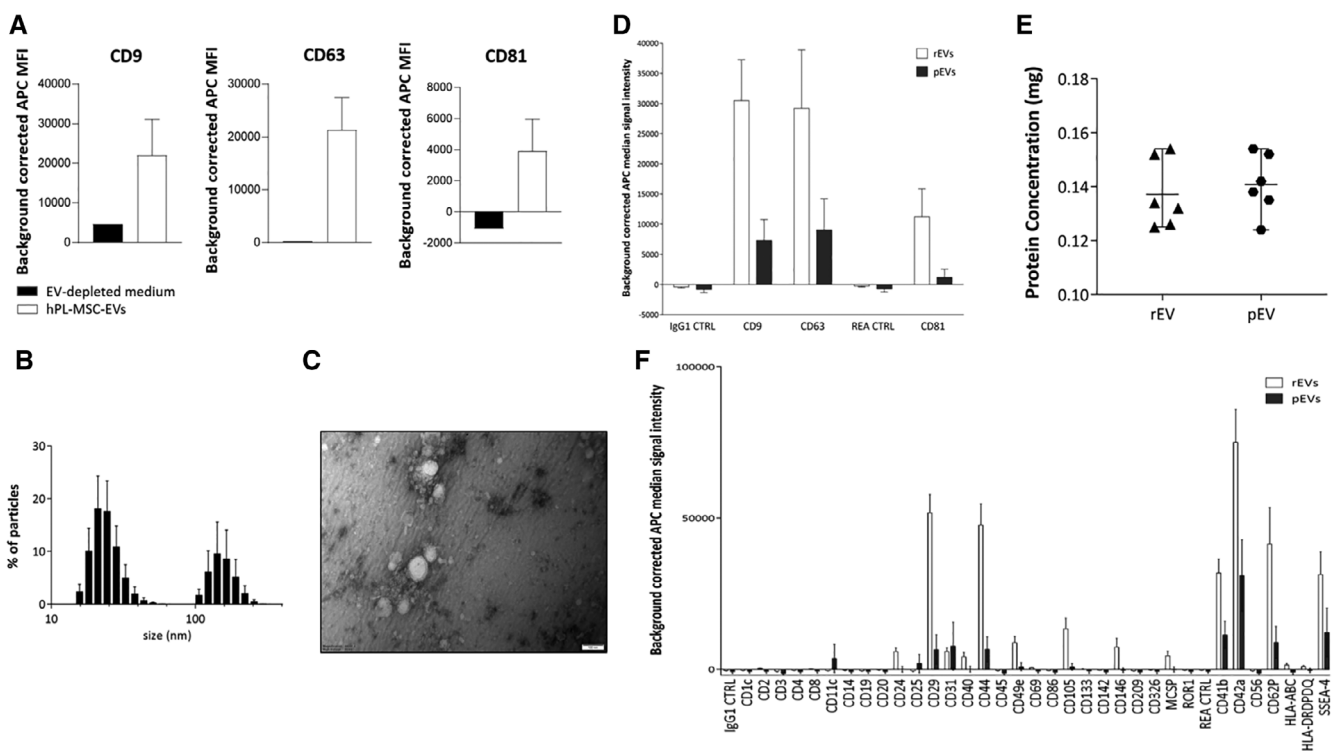


**FIGURE 2** Size, surface marker characterization, and protein quantification of hPL-hBM-MSC-derived EVs. A, Background-corrected median fluorescence intensity of CD9, CD63, and CD81 markers in EV-depleted medium and hPL-hBM-MSC-EVs assessed by FACS. B, Hydrodynamic diameter distribution plots measured on EVs freshly isolated from hPL-hBM-MSCs. Exosomes are represented by the smallest sizes on the left, ranging from 25 to 90 nm, whereas microvesicles by the largest sizes on the right, ranging from 100 to 500 nm. Error bars represent mean  $\pm$  SEM obtained from at least five measurements of six independent samples. All experiments were performed in PBS at  $25^{\circ}\text{C}$ . C, Wide-field TEM image of hPL-MSC-EVs revealing the abundance of EVs. Scale bar: 100 nm. D, Background corrected median fluorescence intensity of CD9, CD63, CD81 markers, and corresponding isotype controls on rEVs and pEVs ( $n = 5$  and  $n = 3$ , respectively). E, EVs were isolated from six different treated hPL-hBM-MSCs (pEVs) or not treated (rEVs) with  $\text{IFN-}\gamma$  (10 ng/mL) and  $\text{TNF-}\alpha$  (15 ng/mL) for 48 hours. Scatter plot shows the absolute protein concentration of rEVs (on the left) and pEVs (on the right), through BCA protein assay. Error bars represent mean  $\pm$  SEM obtained from at least six independent samples. F, Background-corrected median fluorescence intensity of 36 surface epitopes on rEVs and pEVs ( $n = 5$  and  $n = 3$ , respectively). BCA, bichinoninic acid; EVs, extracellular vesicles; hBM-MSCs, human bone marrow-derived MSCs; hPL, human platelet lysate; MSCs, mesenchymal stromal cells; TEM, transmission electron microscopy

hPL-hBM-MSC-EVs, isolated through ultracentrifugation from the supernatant of cells cultured in EV-free conditioned medium,<sup>30</sup> we could recognize exosomes, ranging 25-90 nm, and microvesicles, ranging 100-500 nm (Figure 2B). To confirm the presence of EVs obtained from cell culture media, an aliquot of resuspended hPL-MSC-EVs was visualized by using transmission electron microscopy (TEM). An abundance of particles with the expected diameter and morphology of EVs was present (Figure 2C). The spherical appearance of these particles suggested that they maintained their integrity following the isolation process. As also confirmed by DLS measurements, qualitative assessment of TEM images suggested that most of the isolated EVs fell within the exosome size range, whereas EVs with the microvesicle size range were less frequent. Both resting- (rEVs) and primed-EVs (pEVs) showed similar protein concentration according to the BCA Protein Assay (Figure 2D). Further characterization includes the assessment of the EV surface marker profile by using a multiplex bead-based platform (Figure S3B). Both rEVs and pEVs were positive for the exosome markers including CD63, CD9, and CD81 (Figure 2E). EVs were also positive for CD29, CD44, CD105 (Figure 2F). As previously observed for FBS-hBM-MSC-EVs,<sup>33</sup> hPL-hBM-MSC-EVs expressed SSEA-4, an early embryonic glycolipid antigen identifying the adult MSC population derived from BM,<sup>45</sup>

and CD146, characterizing a specific subpopulation of MSCs with high therapeutic potential.<sup>46</sup> In summary, hPL-hBM-MSC-EVs are very similar to FBS-hBM-MSC-EVs in terms of size, surface expression markers, and protein content, thus suggesting that hPL-supplemented medium does not modify significantly the molecular, proteomic, and immunological properties of hBM-MSC-EVs.

### 3.3 | T-reg induction mediates EV immunomodulatory effect in vitro

The ability of hBM-MSCs to drive CD4<sup>+</sup> T-cell functional switch toward the T-reg phenotype (CD4<sup>+</sup>CD25<sup>+</sup>CD127<sup>low</sup>FoxP3<sup>+</sup>) has been previously reported.<sup>46</sup> EV-mediated immune regulation seems to be particularly related to reduce proliferation of B- and NK-cells, rather than T-cell proliferation.<sup>30</sup> However, our group has previously described in vitro a relative increase in CD4<sup>+</sup> T-cell population following the co-culture with EVs.<sup>30</sup> Here, we assessed the effect of rEVs and pEVs on T-cells, by measuring the phenotypic switch of CD4<sup>+</sup> T-cells toward T-regs. We tested on activated T-cells the effect of increasing quantities of EVs, as assessed by protein concentration

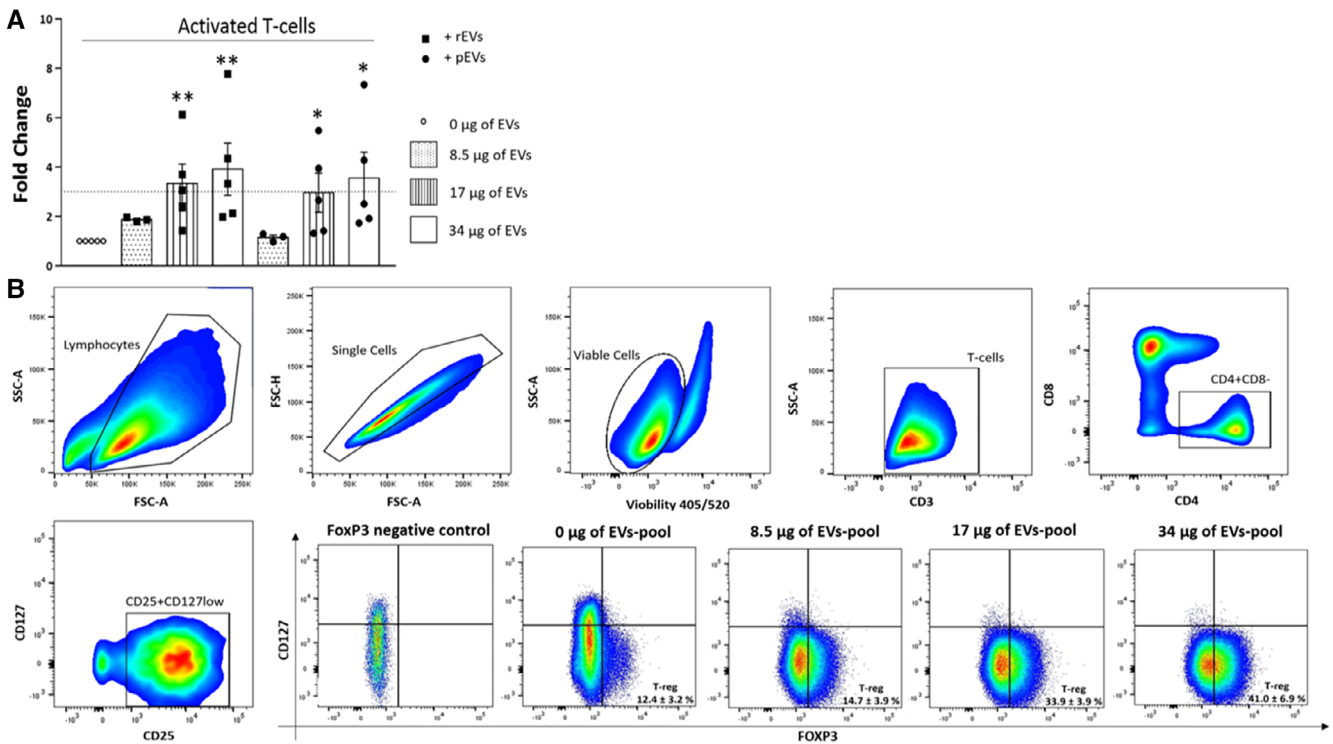


**FIGURE 3** In vitro assay and gating strategy to study the induction of EV-mediated T-regulatory cells. A,  $2 \times 10^5$  activated T-cells were co-cultured for 7 days in the presence or not of different amount of rEVs and pEVs in terms of protein concentration (8.5, 17, and 34  $\mu$ g). Then, T-reg induction was evaluated through FACS analysis. The histogram shows the T-reg proportion (calculated as the percentage of CD4<sup>+</sup>CD25<sup>+</sup>CD127<sup>low</sup>FoxP3<sup>+</sup> cells on CD4<sup>+</sup> cells and normalized on untreated T cells) following the treatment with rEVs and pEVs. Data were compared using Student's unpaired t tests. Error bars represent mean  $\pm$  SEM obtained from at least each measurement of three (for 8.5  $\mu$ g) or five (for 17 and 34  $\mu$ g) independent experiments. \* $P < .05$ , \*\* $P < .01$ . B, Gating strategy for evaluating T-reg proportion in the presence or not of rEVs and pEVs. CD3<sup>+</sup> and the subset of CD4<sup>+</sup> cells were gated on lymphocyte population. T-regs were defined as CD4<sup>+</sup>CD25<sup>+</sup>CD127<sup>low</sup>FOXP3<sup>+</sup> T-cells. The last four scatter plots show the representative percentages of T-regs, calculated on CD4<sup>+</sup> cells, following the addition of different EV concentrations (8.5, 17, and 34  $\mu$ g). EVs, extracellular vesicles



(0, 8.5, 17, and 34  $\mu\text{g}$ ), obtained from single-donor hPL-hBM-MSCs. After 7 days of co-culture, FACS analysis demonstrated that EVs were capable of inducing a relative increase in T-reg population (Figure 3A). A significant increase of the proportion of T-regs was observed with both rEVs ( $1.88 \pm 0.09$ ,  $3.77 \pm 2.35$ , and  $4.88 \pm 2.90$  at 8.5, 17, and 34  $\mu\text{g}$  EV protein concentration, respectively) and pEVs ( $1.13 \pm 0.16$ ,  $3.40 \pm 2.08$ , and  $4.54 \pm 2.80$  at 8.5, 17, and 34  $\mu\text{g}$  EV protein concentration, respectively) compared with the control (activated T-cells without EV addition—0  $\mu\text{g}$  EVs) (Figure 3A). Notably, despite the increasing EV concentration, T-reg induction reached a plateau at around threefold increase. These findings suggest that T-reg induction plays a role in the immune regulatory effect of EVs on T-cells, and a cutoff value of threefold increase of T-reg population may be used in vitro as surrogate of EV immunological activity.

### 3.4 | Standardization of aGvHD mouse model to assess in vivo the effectiveness of EV administration

Before performing in vivo experiments, we determined by FACS analysis, a median composition of each PBMC batch, with the

following results:  $81\% \pm 9\%$  for T-cells,  $5.5\% \pm 3.5\%$  for B-cells, and  $9\% \pm 4\%$  for NK-cells, as expected in healthy donors (Figure S4A). Activated T-cells showed a proliferation rate over 90% compared with unstimulated PBMCs, as assessed by CFSE assay (Figure S4B). Based on these in vitro data, NOG mice were treated with sublethal total body irradiation (TBI) and intravenously injected with human PBMCs, as described above. Mice were then individually scored twice a week according to three clinical parameters (posture, activity, fur) on a scale ranging from 0 to 2 (Table 1). Figure 4A summarizes the relative weight loss following PBMC inoculation until day +30, compared with the control group (PBS-only mice). Acute GvHD started at day +9 in aGvHD mouse group (PBMCs 1-5), whereas control mice showed rapid weight recovery and then progressive gain until the end of the experiment (Figure 4A). A significant mortality rate occurred in aGvHD mice between days +12 and +17, particularly at days +13/+14, when the maximum aGvHD clinical score was observed (Figure 4B). A significant infiltration of human  $\text{CD45}^+$  cells, mostly  $\text{CD3}^+$  T-cells, was revealed in aGvHD mouse organs and tissues (BM, lung, liver, spleen, kidney, PB) by FACS analysis and immunohistochemistry (Figure 4C and Figure 5A). Remarkably, spleen size was significantly increased in aGvHD mice

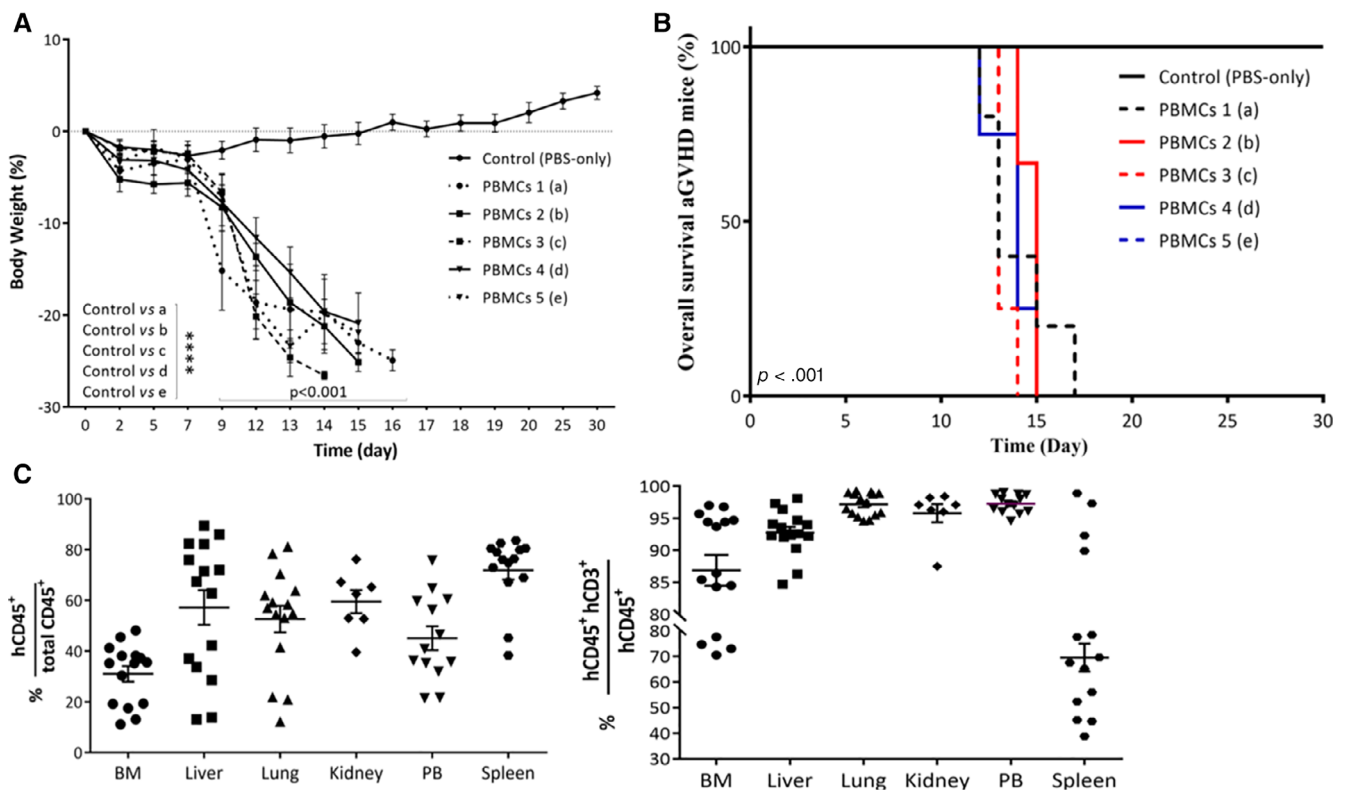


**FIGURE 4** Grading of aGvHD mouse model. A, Weight change curves of aGvHD mice (PBMCs 1-5,  $n = 5$ ) and control mice (PBS-only,  $n = 5$ ). Data were compared using Student's unpaired  $t$  tests and multiple  $t$  tests. B, Kaplan-Meier survival curves of aGvHD mice (PBMCs 1-5,  $n = 5$ ) and control mice (PBS-only,  $n = 5$ ). Log-rank (Mantel-Cox) test was used for statistical analysis. \*\*\*\* $P < .0001$ . Data were obtained with five independent experiments. C, Human infiltrating cells (left) in different mouse target organs ( $n = 5$ ). Data are represented as the percentage of human ( $\text{hCD45}^+$ ) cells on total  $\text{CD45}^+$  cells including mouse cells ( $\text{hCD45}^+$  and  $\text{mCD45}^+$  cells). Error bars represent mean  $\pm$  SEM of three independent experiments. Human infiltrating T-cells (right) in different mouse target organs ( $n = 5$ ). Data are represented as percentage of  $\text{hCD3}^+$  cells on  $\text{hCD45}^+$  cells. Error bars represent mean  $\pm$  SEM of three independent experiments. aGvHD, acute graft-vs-host-disease; PBS, phosphate-buffered saline; PBMCs, peripheral blood mononuclear cells

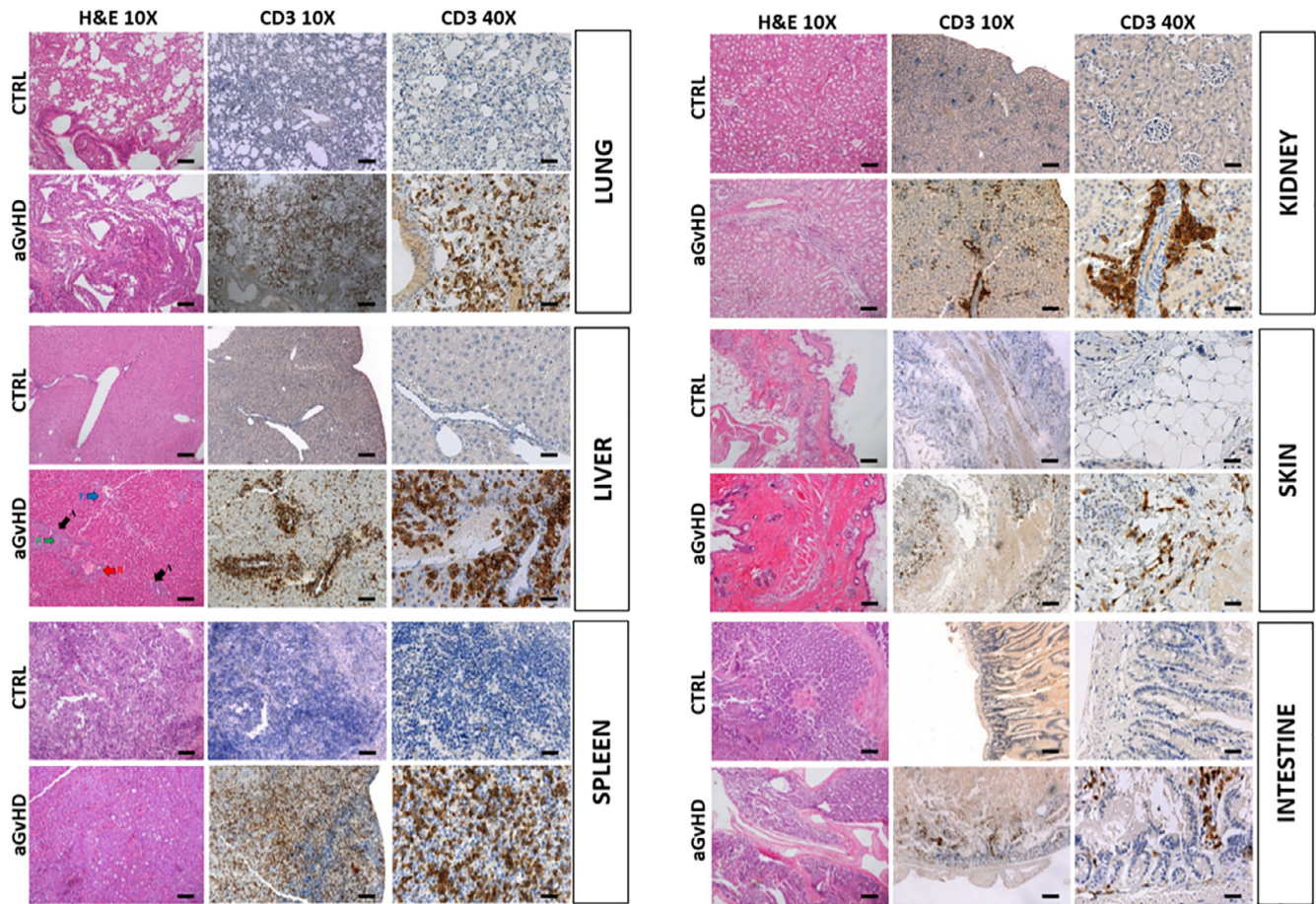


**FIGURE 5** Histopathological evaluation of mouse tissues. Tissues from aGvHD or control (CTRL) mice (lung, liver, spleen, intestine, skin, and kidney) were fixed and stained with Hematoxylin and Eosin or anti-hCD3 to evaluate tissue damage and T-cell infiltration, respectively. Black arrow A = apoptosis, red arrow B = biliary damage, arrow green P = portal infiltrate, blue arrow E = endotheliitis. Scale bars: Low magnification 200  $\mu$ m; high magnification 50  $\mu$ m. aGvHD, acute graft-vs-host-disease

compared with control (Figure S4C). Immunohistochemistry analysis displayed a less broad T-cell infiltration in skin and small intestine, whereas in the liver, portal lymphocytic infiltration, endotheliosis, hepatocyte apoptosis, and biliary duct, damages were evident (Figure 5A). The histopathologic score was used to quantify aGvHD severity (Table 2) since the parameters described in Table 3. All these data confirmed that our mouse model mimic human severe aGvHD in a reproducible manner.

### 3.5 | Definition of in vitro EV-IFU and in vivo EV-TD of hPL-hBM-MS-C-derived EVs

On the basis of in vitro data (Figure 3A) and the absence of significant differences between rEVs and pEVs, particularly as far as T-reg induction is concerned (Figure 3A), we tried to identify a reproducible approach to define the EV-IFU capable of producing a significant immunomodulatory effect in vitro. To reduce the intrinsic variability of single-donor EVs, we adopted an EV-pooling approach by isolating and

pooling rEVs from five donor-hPL-hBM-MS-Cs cultured in the EV-free conditioned medium.<sup>30</sup> Next, we analyzed the capabilities of EV pools to promote T-reg induction in the same condition of protein concentration, as described above (0, 8.5, 17, and 34  $\mu$ g) with single donor rEV (Figure 3A). According to our in vitro data on T-reg induction EVs (Figure 3A), we defined EV-IFU as the lowest concentration of each rEV-pool leading in vitro to at least threefold increase of T-reg compared with controls. In other words, we assumed that different rEV pools from different donors may have the same EV-IFU, and therefore the same reproducible immune regulatory activity, although their protein concentration is different, thus focusing our selection on biological effects rather than protein concentration. Accordingly, we identified three suitable rEV-pools displaying EV-IFU (1 with 17  $\mu$ g and 2 with 34  $\mu$ g proteins each). They were subsequently used for in vivo experiments in aGvHD mice (Figure 6A, red dots).

To assess the therapeutic efficacy of the rEV-pools in vivo, a total dose equal to 10-fold the in vitro EV-IFU was split into three different doses and administered to aGvHD mice at day +1, +4, and +7, thus representing the EV-TD. Mice injected with human PBMCs to induce

**TABLE 2** Histopathological score of organs from treated acute graft-vs-host disease (aGvHD) mice (C-M, n = 11) and control mice (PBS-only, A and B, n = 2), used to evaluate the aGvHD severity evaluated at high magnification

	Lung		Liver				Spleen	Kidney	Skin	Intestine
	Inflammation	Inflammation	Inflammation	Biliary damage	Centrilobular vein endothelitis	Apoptosis				
A	0	0	0	0	0	0	0	0	0	0
B	0	0	0	0	0	0	0	0	0	0
C	2	3	3	3	1	3	2	3	1	1
D	4	4	4	4	2	3	4	4	2	3
E	1	1	1	0	0	0	2	0	0	1
F	2	2	2	1	0	1	3	1	0	1
G	1	1	1	1	0	0	3	1	0	0
H	2	2	2	2	1	1	3	2	0	1
I	4	3	3	3	3	3	3	3	1	2
J	4	4	4	4	3	3	4	3	1	1
K	3	3	3	2	3	1	2	1	1	1
L	4	3	3	3	3	3	3	2	1	1
M	3	3	3	2	2	3	3	3	1	1

**TABLE 3** Histologic scoring (0-4) of lung, liver, spleen, kidney, skin, and intestine of aGvHD mice based on histopathological evaluation of mouse tissues at high magnification

Organs	Damage	Score	
Lung, spleen, kidney	Inflammation	0 No infiltration	
		1 Sporadic or <5% infiltration	
		2 Mild infiltration of 5%-25%	
		3 Moderate infiltration of 25%-50%	
	4 Severe infiltration of >60%		
Liver	Portal infiltrate	0 None	
		1 Mild, some, or all portal areas	
		2 Moderate, some, or all portal areas	
		3 Moderate/marked, all portal areas	
		4 Marked, all portal areas	
	Biliary damage	0 Absent	
		1 Minimal	
		2 Mild and diffuse	
		3 Moderate	
		4 Severe with new small bile duct present in all portal area	
	Centrilobular vein endotheliitis	0 Normal (occasional lymphocytes around portal triads are acceptable)	
		1 Rare (1-2/0.5 cm) focal collections of mononuclear cells in parenchyma)	
2 Endotheliosis present in one vessel/0.5 cm (subendothelial infiltrate of a depth at least two cells in one vessel)			
3 Endotheliosis present in >3 vessels/0.5 cm with the infiltrating depth >3 cells			
	4 Endotheliosis as above present in virtually all vessels		
Apoptosis	0 Absent		
	1 Minimal (<2 foci 10x)		
	2 Moderate (2-4 foci 10x)		
	3 Severe (>5 foci 10x)		
Skin	Inflammation	0 None	
		1 Focal infiltrates	
		2 Widespread infiltrates	
Small intestine	Inflammation	0 None	
		1 Mild	
		2 Moderate	
		3 Severe without ulceration	
		4 Severe, with ulceration	

Abbreviation: aGvHD, acute graft-vs-host-disease.

aGvHD and treated with EV-TD (EV-TD mice) were compared with controls, that is, untreated aGvHD mice (EV-UT mice) receiving three doses of PBS only. At day +9 and +12, the number of human T-reg,



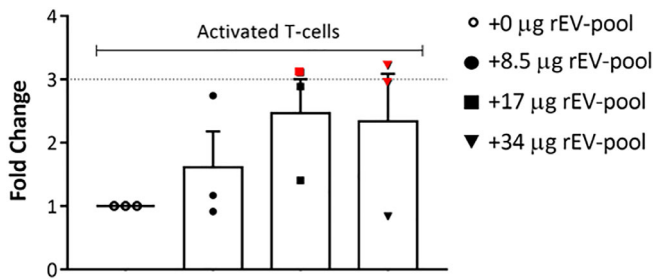


**FIGURE 6** Definition of therapeutic protocol for in vivo experiments. Representative graph to define the in vitro EV-IFU:  $2 \times 10^5$  activated T-cells ( $0.5 \mu\text{g/mL}$  anti-CD3 and  $0.5 \mu\text{g/mL}$  anti-CD28 antibodies) were co-cultured for 7 days with different rEV-pools at three different EV concentrations (8.5, 17, and  $34 \mu\text{g}$ ). The red spots display the rEV-pools increasing at least threefold the number of T-regs compared with the control (activated T-cells without EV addition,  $0 \mu\text{g}$  of rEV-pool). These three suitable rEV-pools (one with  $17 \mu\text{g}$  and two with  $34 \mu\text{g}$  proteins each) were then used for in vivo experiments in aGvHD mice. Error bars represent mean  $\pm$  SEM of three independent experiments. aGvHD, acute graft-vs-host-disease; EV, extracellular vesicle; EV-IFU, EV immunomodulatory functional unit

CD4<sup>+</sup>, and CD8<sup>+</sup> T-cells in mouse PB as well as at day +9 the plasma levels of human cytokines, such as TNF- $\alpha$  and IFN- $\gamma$ , were measured. We then monitored aGvHD onset and progression through several clinical parameters (Table 1), weight loss, and overall survival. Such therapeutic schedule significantly improved the overall survival of EV-TD mice compared with EV-UT mice (Figure 7A); none of the EV-UT mice survived beyond day +17, whereas EV-TD mice were still alive until day +28 (Figure 7A). In addition, EV-TD administration hampered significantly the onset of aGvHD clinical signs, reducing the weight loss (11.5% in the EV-TD mice vs 19.5% in EV-UT mice at day +13, \*\* $P < .01$ ) (Figure 7B). No significant changes were observed in the histopathologic score of the EV-TD mouse organs compared with the EV-UT ones (data not shown). These findings are in line with those recently shown by other authors<sup>47</sup> and are related to the short follow-up of the experimental plan that was mainly aimed at quantifying reproducibly the effectiveness of EV administration schedule. Nevertheless, i.v. administration of EV-TD was associated with the temporary increase of circulating T-regs as well as of the plasmatic levels of TNF- $\alpha$  and IFN- $\gamma$ , that is, the cytokine involved in both EV immunomodulation<sup>48,49</sup> and T-reg expansion.<sup>50</sup> In fact, at day +9, that is, 2 days after the administration of the last dose of EV-TD, T-regs were significantly increased in PB of EV-TD compared with EV-UT mice, whereas at day +12, the two groups showed similar T-reg levels (Figure 7C). In addition, at day +9, the plasma levels of human TNF- $\alpha$  and IFN- $\gamma$  were significantly increased in EV-TD mice compared with EV-UT mice (TNF- $\alpha$ :  $67.45 \pm 24.01 \text{ pg/mL}$  in EV-TD mice vs  $39.55 \pm 15.36 \text{ pg/mL}$  in EV-UT mice; IFN- $\gamma$ :  $7.43 \pm 2.86 \text{ pg/mL}$  in EV-TD mice vs  $5.21 \pm 1.12 \text{ pg/mL}$  in EV-UT mice, respectively) (Figure 7D). Nonetheless, i.v. administration of EV-TD was associated to a nonsignificant modulation of circulating CD4<sup>+</sup> and CD8<sup>+</sup> T-cells (CD3<sup>+</sup>CD4<sup>+</sup>:  $1.33 \pm 1.28$  and  $1.18 \pm 0.9$ , CD3<sup>+</sup>CD8<sup>+</sup>:  $0.83 \pm 0.55$  and  $0.93 \pm 0.85$  at days 9 and 12, respectively) (Figure S5).

## 4 | DISCUSSION

In 2014 a compassionate case of severe therapy-refractory aGvHD, affecting about 30% of the Allo-HSCT patients, was treated with MSC-derived EVs of four different BM-unrelated donors. The patient recovered within a few months after repeated treatments, suggesting that MSC-derived EVs could provide a potential cell-free and safe tool to treat severe aGvHD and other inflammatory diseases.<sup>51</sup> Further evidence of aGvHD improvement following therapeutic infusion of hBM-MSC-EVs, possibly due to their peculiar microRNA profiles, was recently published,<sup>47</sup> suggesting that hBM-MSC-EVs represent a potential answer for important issues related to MSC clinical use. In fact, although MSCs have been proven to be effective in treating refractory aGvHD,<sup>15</sup> their immune regulatory properties are hardly predictable in vivo for several intrinsic and extrinsic reasons. Different MSC tissue origin, concentration, dose number, administration route, and timing as well the inflammatory status of the recipient may lead to opposite results in terms of efficacy, thus questioning in some cases the validity of their clinical use.<sup>52,53</sup>

Conversely, the use of MSC-derived EVs to prevent and treat steroid-refractory aGvHD provides several potential advantages compared with whole MSC administration.<sup>38</sup> Although they contain high concentrations of proteins and nucleic acids, including DNA and different RNA types, acting as powerful regulators of many cell functions, EVs are cell particles devoid of autonomous replication and therefore of neoplastic transformation risk.<sup>29</sup> In addition, EVs can be sterilized by filtration due to their small size and, theoretically, it is possible to harvest EVs even from supernatants of immortalized MSC cell lines, which otherwise could not be used for cellular therapies.<sup>51</sup> Thus, the regulatory issues to produce EVs for clinical purposes can be less complicated than for any other cellular strategy based on ex vivo cell expansion and systemic administration into patients.<sup>51</sup>

Unfortunately, so far, the main challenge remains the precise characterization of the therapeutic EV content as well as the definition of the effective EV dose before infusion to predict the clinical benefit with good approximation. Even though hBM-MSC-EVs display many of the BM-MSC immune regulatory properties, their content in paracrine factors greatly varies according to the techniques used for EV separation and the activation status of MSCs.<sup>31,32</sup> Differential ultracentrifugation (with or without immunomagnetic selection) is commonly used to characterize all the EVs released by MSCs, including small and large vesicles, and to obtain a final product devoid of additional chemicals that could influence both functional studies and clinical application.<sup>54</sup> Several other EV-selecting platforms have been developed, such as immunomagnetic exosome RNA analysis, miniaturized micro-nuclear magnetic resonance microfluidic chip system, Exochip, label-free high-throughput nano-plasmonic exosome assay using surface plasmon resonance and other procedures. Nevertheless, most of the studies on the EV biological activities are still based on indirect in vitro evidence, especially in the context of the immune system.<sup>32</sup> This issue has triggered many different attempts to define reliable assays for characterizing the functionality of MSC-EV preparations prior to administration into patients.<sup>37</sup>



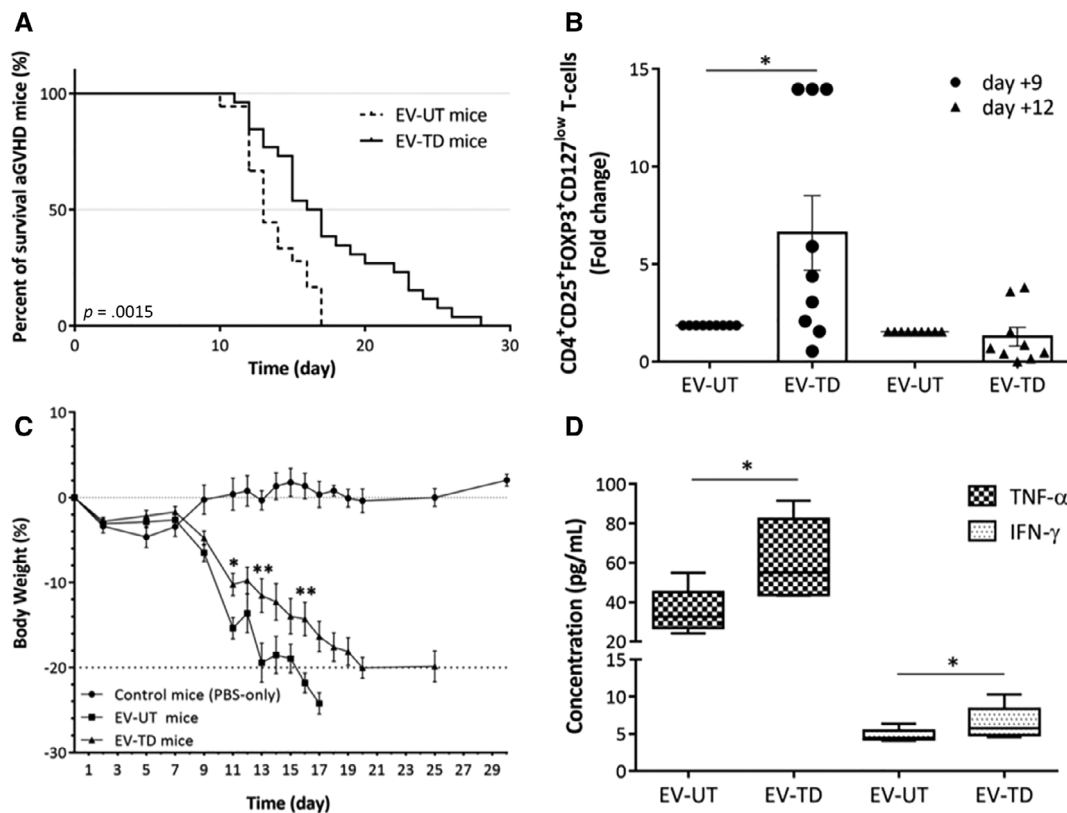


**FIGURE 7** Monitoring the effect of EV treatment in vivo. A, Kaplan-Meier survival curves of EV-UT mice (untreated aGvHD mice,  $n = 6$ ) and EV-TD mice (aGvHD mice treated with EV-TD,  $n = 8$ ). Log-rank (Mantel-Cox) test was used for statistical analysis. Data were obtained with three independent experiments. B, Weight change curves of control mice (PBS-only,  $n = 1$ ), EV-UT mice (untreated aGvHD mice,  $n = 8$ ) and EV-TD mice (aGvHD mice treated with EV-TD,  $n = 10$ ). Data were compared using Student's unpaired  $t$  tests and multiple  $t$  tests. Error bars represent mean  $\pm$  SEM obtained from five independent experiments. C, Peripheral blood T-reg evaluation was performed after 9 and 12 days from PBMC inoculation in the aGvHD mouse model. EV-TD mice ( $n = 3$ ) were treated three times (day +1, +4 and +7) with EV-TD; EV-UT mice ( $n = 3$ ) received only vehicle (PBS). FACS analysis was performed by  $CD4^+CD25^+CD127^{low}FOXP3^+$  gating on T-cells. Error bars represent mean  $\pm$  SEM obtained from three independent experiments. Data were compared using Student's unpaired  $t$  tests. D, Quantikine ELISA was performed on plasma samples at +9 days from PBMC inoculation into aGvHD mouse model (EV-UT and EV-TD,  $n = 5$  each). Error bars represent mean  $\pm$  SEM obtained from at least five measurements of independent samples. Data were compared using Student's unpaired  $t$  tests. \* $P < .05$ , \*\* $P < .01$ . aGvHD, acute graft-vs-host-disease; EV, extracellular vesicle; EV-TD, EV treated; EV-UT, EV-untreated; PBS, phosphate-buffered saline; PBMCs, peripheral blood mononuclear cells

In this study, we established a simple method to characterize reproducibly the EV immune regulatory activity according to their capability to induce in vitro and in vivo a specific immunological effect that is important for aGvHD amelioration, that is, T-reg induction,<sup>55</sup> rather than on the basis of their protein content and concentration. In fact, the simple protein quantification does not reflect the measurable biological effects, because the protein content may vary qualitatively according to many factors related to donor or expansion procedures. This evidence explains the resulting heterogeneity described in the literature. Therefore, considering the well-known limitations of considering only protein concentration for EVs quantification, we suggested a more reliable method of EV quantification by combining their protein concentration with a biomarker of their biological activity (T-reg induction). We found that this immunomodulatory mechanism is displayed by both rEVs (from resting hPL-BM-MSCs) and pEVs (from inflammatory-primed hPL-BM-MSCs), even though their surface epitopes are differentially expressed and their protein content does not vary significantly. In other words, we focused our

attention only on EV biological effects by assuming that different rEV-pools from different donors may have the same reproducible immune regulatory activity, although their protein concentration may be different due to the intrinsic variability of single-donor EVs. To this aim, we chose some experimental approaches that have been standardized: (i) we adopted an EV-pooling protocol by isolating rEVs through ultracentrifugation from five donor-hPL-hBM-MSCs cultured in EV-free conditioned medium, rather than using a fixed protein concentration of single-donor hBM-MSC-EVs; (ii) we previously assessed that the EVs used for in vitro and in vivo immunological assays were from hBM-MSCs that were proved effective in vitro in terms of IEC inhibition and T-reg induction. Therefore, we eventually chose and characterized hPL-hBM-MSC-EVs, due to the advantages in terms of MSC expansion yield and safety with the same immunoregulatory properties; (iii) we developed a very efficient xenogeneic NOG mouse model capable to mimic human severe aGvHD in a reproducible manner, with the maximum aGvHD clinical score at days +13/+14, easily measurable by both clinical and

histopathological parameters, and the maximum mortality rate between day +12 and +17.

We then applied the above-mentioned strategy and read-out to assess in vitro and in vivo the effectiveness of the use of hPL-hBM-MS-C-derived rEV-pools. Thus, we could first quantify reproducibly the rEV-pool immunomodulatory effect in vitro in terms of EV-IFU. This was the prerequisite to select only those EV pools mediating the beneficial effect, regardless of their protein concentration and according to the results obtained with single donor-derived hPL-hBM-MS-C-EVs showing at least threefold T-reg increase compared with controls. Consequently, we could establish empirically the EV-TD corresponding to 10-fold the in vitro EV-IFU, taking into consideration that many interfering factors following EV administration in vivo may influence and bias the final clinical effect in patients (drug interactions, inflammatory status, lymphocytopenia, concomitant infections, etc). According to this approach, we observed a significant improvement of both mouse overall survival and aGvHD amelioration in terms of clinical scores. As expected,<sup>47</sup> the short follow-up did not allow us to find significant differences in terms of histopathological score; nevertheless, we observed the parallel increase of some biomarkers, such as circulating T-regs and plasmatic cytokines playing a role in T-reg induction and EV immunomodulation (TNF- $\alpha$  and IFN- $\gamma$ ).<sup>48,55,56</sup>

## 5 | CONCLUSION

In summary, our mouse model of aGvHD suggests that EVs may represent a safe and valid alternative to whole MSCs for patients with steroid-refractory aGvHD. The effective dose of EV pools is reproducibly identified according to EV-IFU and EV-TD definition, with a number of advantages in terms of patient's safety, availability, quantification of biological effects, and reproducibility. An administration schedule based on repeated administration EV-TD and with a longer follow-up will help to clarify the clinical impact of this experimental approach in aGvHD also in terms of prevention of histopathological damages and long-term survival.

## ACKNOWLEDGMENTS

This work was supported by Fondazione Cassa di Risparmio di Verona Vicenza Belluno e Ancona. The study was conducted in Interdepartmental Laboratory of Medical Research (LURM) at the University of Verona, Verona, Italy. We would like to thank: Centro Piattaforme Tecnologiche and the Pathology Unit, University of Verona, for their contribution and help in DLS and TEM, and immunohistochemistry, respectively; Laboratorio di Terapie Cellulari Avanzate, Ospedale San Bortolo, Vicenza (Italy) for quality assays on hPL supplement; Unità Semplice di Genetica Medica, AOUI, Verona for the help in karyotyping; Chiasseu Marius Trésor from Yale School of Medicine, New Haven, Connecticut, for English support.

## CONFLICT OF INTEREST

The authors indicated no potential conflicts of interest.

## AUTHOR CONTRIBUTIONS

G.D.C., A.A.: collection and assembly of data, data analysis and interpretation, manuscript writing; A.G.: conception and design, collection and assembly of data, data analysis and interpretation; E.T.: collection and assembly of data, manuscript writing; R.B., F.M.Q.: collection and assembly of data; P.T.K.: conception and design, data analysis and interpretation, manuscript writing; C.T.: provision of study material, manuscript writing; M.K.: conception and design, financial support, provision of study materials, manuscript writing, final approval of the manuscript.

## DATA AVAILABILITY STATEMENT

The data that support the findings of this study are available from the corresponding author upon reasonable request.

## ORCID

Giada Dal Collo  <https://orcid.org/0000-0001-7348-370X>

## REFERENCES

1. Ghimire S et al. Pathophysiology of GvHD and other HSCT-related major complications. *Front Immunol.* 2017;8:79-79.
2. Inamoto Y, Flowers MED. Treatment of chronic graft-versus-host-disease in 2011. *Curr Opin Hematol.* 2011;18(6):414-420.
3. Kuba A, Raida L. Graft versus host disease: from basic pathogenic principles to DNA damage response and cellular senescence. *Mediators Inflamm.* 2018;2018:9451950.
4. Santos E, Sousa P, Bennett CL, Chakraverty R. Unraveling the mechanisms of cutaneous graft-versus-host disease. *Front Immunol.* 2018;9:963.
5. Lee SJ. Classification systems for chronic graft-versus-host disease. *Blood.* 2017;129(1):30-37.
6. Nassereddine S et al. Acute graft versus host disease: a comprehensive review. *Anticancer Res.* 2017;37(4):1547-1555.
7. Funke VAM, Moreira MCR, Vigorito AC. Acute and chronic graft-versus-host disease after hematopoietic stem cell transplantation. *J Revista da Associação Médica Brasileira.* 2016;62:44-50.
8. Schoemans HM et al. EBMT-NIH-CIBMTR task force position statement on standardized terminology & guidance for graft-versus-host disease assessment. *Bone Marrow Transplant.* 2018;53(11):1401-1415.
9. Murray J, Stringer J, Hutt D. Graft-versus-host disease (GvHD). In: Kenyon M, Babic A, eds. *The European Blood and Marrow Transplantation Textbook for Nurses: Under the Auspices of EBMT.* Cham, Switzerland: Springer International Publishing; 2018: 221-251.
10. MacDonald KPA, Hill GR, Blazar BR. Chronic graft-versus-host disease: biological insights from preclinical and clinical studies. *Blood.* 2017;129(1):13-21.
11. Hill L et al. New and emerging therapies for acute and chronic graft versus host disease. *Ther Adv Hematol.* 2018;9(1):21-46.
12. Fløisand Y et al. Safety and effectiveness of Vedolizumab in patients with steroid-refractory gastrointestinal acute graft-versus-host disease: a retrospective record review. *Biol Blood Marrow Transplant.* 2019;25(4):720-727.
13. Palmer J et al. Predictors of survival, nonrelapse mortality, and failure-free survival in patients treated for chronic graft-versus-host disease. *Blood.* 2016;127(1):160-166.
14. Le Blanc K et al. Treatment of severe acute graft-versus-host disease with third party haploidentical mesenchymal stem cells. *Lancet.* 2004; 363(9419):1439-1441.

15. Le Blanc K et al. Mesenchymal stem cells for treatment of steroid-resistant, severe, acute graft-versus-host disease: a phase II study. *Lancet*. 2008;371(9624):1579-1586.
16. Elgaz S et al. Clinical use of mesenchymal stromal cells in the treatment of acute graft-versus-host disease. *Transfus Med Hemother*. 2019;46(1):27-34.
17. Galipeau J, Sensébé L. Mesenchymal stromal cells: clinical challenges and therapeutic opportunities. *Cell Stem Cell*. 2018;22(6):824-833.
18. Sudres M et al. Bone marrow mesenchymal stem cells suppress lymphocyte proliferation in vitro but fail to prevent graft-versus-host disease in mice. *J Immunol*. 2006;176(12):7761-7767.
19. Yañez R et al. Adipose tissue-derived mesenchymal stem cells have in vivo immunosuppressive properties applicable for the control of the graft-versus-host disease. *STEM CELLS*. 2006;24(11):2582-2591.
20. Auletta JJ et al. Human mesenchymal stromal cells attenuate graft-versus-host disease and maintain graft-versus-leukemia activity following experimental allogeneic bone marrow transplantation. *STEM CELLS*. 2015;33(2):601-614.
21. Figueroa FE et al. Mesenchymal stem cell treatment for autoimmune diseases: a critical review. *J Biol Res*. 2012;45:269-277.
22. Gregoire C et al. Comparison of mesenchymal stromal cells from different origins for the treatment of graft-vs.-host-disease in a humanized mouse model. *Front Immunol*. 2019;10:619.
23. Seng A, Dunavin N. Mesenchymal stromal cell infusions for acute graft-versus-host disease: rationale, data, and unanswered questions. *Adv Cell Gene Ther*. 2018;1(2):e14.
24. Baron F, Storb R. Mesenchymal stromal cells: a new tool against graft-versus-host disease? *Biol Blood Marrow Transplant*. 2012;18(6):822-840.
25. Bianco P, Robey PG, Simmons PJ. Mesenchymal stem cells: revisiting history, concepts, and assays. *Cell Stem Cell*. 2008;2(4):313-319.
26. Greim H et al. The bone marrow niche, stem cells, and leukemia: impact of drugs, chemicals, and the environment. *Ann N Y Acad Sci*. 2014;1310:7-31.
27. Dominici M et al. Minimal criteria for defining multipotent mesenchymal stromal cells. The International Society for Cellular Therapy position statement. *Cytotherapy*. 2006;8(4):315-317.
28. Krampera M. Mesenchymal stromal cell 'licensing': a multistep process. *Leukemia*. 2011;25(9):1408-1414.
29. Adamo A et al. Role of mesenchymal stromal cell-derived extracellular vesicles in tumour microenvironment. *Biochim Biophys Acta rev Cancer*. 2019;1871(1):192-198.
30. Di Trapani M et al. Differential and transferable modulatory effects of mesenchymal stromal cell-derived extracellular vesicles on T, B and NK cell functions. *Sci Rep*. 2016;6:24120.
31. Szatanek R et al. The methods of choice for extracellular vesicles (EVs) characterization. *Int J Mol Sci*. 2017;18(6):E1153.
32. Yanez-Mo M et al. Biological properties of extracellular vesicles and their physiological functions. *J Extracell Vesicles*. 2015;4:27066.
33. Adamo A et al. Extracellular vesicles mediate mesenchymal stromal cell-dependent regulation of B cell PI3K-AKT Signaling pathway and Actin cytoskeleton. *Front Immunol*. 2019;10:446.
34. Pereira LMS et al. Regulatory T cell and Forkhead box protein 3 as modulators of immune homeostasis. *Front Immunol*. 2017;8:605-605.
35. Romano M et al. Past, present, and future of regulatory T cell therapy in transplantation and autoimmunity. *Front Immunol*. 2019;10:43.
36. Kumar S, Mohammadpour H, Cao X. Targeting cytokines in GVHD therapy. *J Immunol Res Ther*. 2017;2(1):90-99.
37. Kordelas L et al. Individual immune-modulatory capabilities of MSC-derived extracellular vesicle (EV) preparations and recipient-dependent responsiveness. *Int J Mol Sci*. 2019;20(7):E1642.
38. Lai P et al. Novel insights into MSC-EVs therapy for immune diseases. *Biomarker Res*. 2019;7:6-6.
39. Hemeda H, Giebel B, Wagner W. Evaluation of human platelet lysate versus fetal bovine serum for culture of mesenchymal stromal cells. *Cytotherapy*. 2014;16(2):170-180.
40. Astori G et al. Platelet lysate as a substitute for animal serum for the ex-vivo expansion of mesenchymal stem/stromal cells: present and future. *Stem Cell Res Ther*. 2016;7(1):93.
41. Wiklander OPB et al. Extracellular vesicle in vivo biodistribution is determined by cell source, route of administration and targeting. *J Extracell Vesicles*. 2015;4:26316-26316.
42. Takam Kanga P et al. Notch signalling drives bone marrow stromal cell-mediated chemoresistance in acute myeloid leukemia. *Oncotarget*. 2016;7(16):21713-21727.
43. Takam Kanga P et al. Inhibition of notch Signaling enhances Chemosensitivity in B-cell precursor acute lymphoblastic Leukemia. *Cancer Res*. 2019;79(3):639-649.
44. Fernandez-Rebollo E et al. Human platelet lysate versus Fetal calf serum: these supplements do not select for different mesenchymal stromal cells. *Sci Rep*. 2017;7(1):5132.
45. Gang EJ et al. SSEA-4 identifies mesenchymal stem cells from bone marrow. *Blood*. 2007;109(4):1743-1751.
46. Wu CC et al. CD146+ mesenchymal stem cells display greater therapeutic potential than CD146- cells for treating collagen-induced arthritis in mice. *Stem Cell Res Ther*. 2016;7:23.
47. Fujii S et al. Graft-versus-host disease amelioration by human bone marrow mesenchymal stromal/stem cell-derived extracellular vesicles is associated with peripheral preservation of naive T cell populations. *STEM CELLS*. 2018;36(3):434-445.
48. Robbins PD, Morelli AE. Regulation of immune responses by extracellular vesicles. *Nat rev Immunol*. 2014;14(3):195-208.
49. Serejo TRT et al. Assessment of the immunosuppressive potential of IFN- $\gamma$  licensed adipose mesenchymal stem cells, their secretome and extracellular vesicles. *Cells*. 2019;8(1):22.
50. Hoepli RE et al. The environment of regulatory T cell biology: cytokines, metabolites, and the microbiome. *Front Immunol*. 2015;6:61-61.
51. Kordelas L et al. MSC-derived exosomes: a novel tool to treat therapy-refractory graft-versus-host disease. *Leukemia*. 2014;28(4):970-973.
52. Sipp D, Robey PG, Turner L. Clear up this stem-cell mess. *Nature*. 2018;561(7724):455-457.
53. Galipeau J, Weiss DJ, Dominici M. Response to nature commentary "clear up this stem-cell mess". *Cytotherapy*. 2019;21(1):1-2.
54. Livshits MA et al. Isolation of exosomes by differential centrifugation: theoretical analysis of a commonly used protocol. *Sci Rep*. 2015;5:17319.
55. Mancusi A et al. The effect of TNF- $\alpha$  on regulatory T cell function in graft-versus-host disease. *Front Immunol*. 2018;9:356-356.
56. Serejo TRT et al. Assessment of the immunosuppressive potential of INF- $\gamma$  licensed adipose mesenchymal stem cells, their secretome and extracellular vesicles. *Cells*. 2019;8(1):22.

## SUPPORTING INFORMATION

Additional supporting information may be found online in the Supporting Information section at the end of this article.

**How to cite this article:** Dal Collo G, Adamo A, Gatti A, et al. Functional dosing of mesenchymal stromal cell-derived extracellular vesicles for the prevention of acute graft-versus-host-disease. *Stem Cells*. 2020;38:698-711. <https://doi.org/10.1002/stem.3160>